

Effects of grain growth mechanisms on the extinction curve and the metal depletion in the interstellar medium

Hiroyuki Hirashita^{1*} and Nikolai V. Voshchinnikov²

¹*Institute of Astronomy and Astrophysics, Academia Sinica, P.O. Box 23-141, Taipei 10617, Taiwan*

²*Sobolev Astronomical Institute, St. Petersburg University, Universitetskii prosp., 28, St. Petersburg 198504, Russia*

2013 October 17

ABSTRACT

Dust grains grow their sizes in the interstellar clouds (especially in molecular clouds) by accretion and coagulation. Here we model and test these processes by examining the consistency with the observed variation of the extinction curves in the Milky Way. We find that, if we simply use the parameters used in previous studies, the model fails to explain the flattening of far-UV extinction curve for large R_V (flatness of optical extinction curve) and the existence of carbon bump even in flat extinction curves. This discrepancy is resolved by adopting a ‘tuned’ model, in which coagulation of carbonaceous dust is less efficient (by a factor of 2) and that of silicate is more efficient with the coagulation threshold removed. The tuned model is also consistent with the relation between silicon depletion (indicator of accretion) and R_V if the duration of accretion and coagulation is $\gtrsim 100(n_H/10^3 \text{ cm}^{-3})^{-1}$ Myr, where n_H is the number density of hydrogen nuclei in the cloud. We also examine the relations between each of the extinction curve features (UV slope, far-UV curvature, and carbon bump strength) and R_V . The correlation between UV slope and R_V , which is the strongest among the three correlations, is well reproduced by the tuned model. For far-UV curvature and carbon bump strength, the observational data are located between the tuned model and the original model without tuning, implying that the large scatters in the observational data can be explained by the sensitive response to the coagulation efficiency. The overall success of the tuned model indicates that accretion and coagulation are promising mechanisms of producing the variation of extinction curves in the Milky Way, although we do not exclude possibilities of other dust-processing mechanisms changing extinction curves.

Key words: dust, extinction — galaxies: evolution — galaxies: ISM — ISM: clouds — ISM: evolution — turbulence

1 INTRODUCTION

The evolution of interstellar dust is one of the most important problems in clarifying the galaxy evolution. The essential features of dust properties are grain size distribution and grain materials. Dust grains actually modify the spectral energy distribution of galaxies by reprocessing stellar radiation into the far-infrared regions in a way dependent on the extinction and the emission cross-section (e.g. Désert, Boulanger, & Puget 1990), both of which are mainly determined by the grain size distribution and the grain materials. Not only radiative processes but also interstellar chemical reactions are affected by dust properties: especially, formation of molecular hydrogen predominantly occurs on dust grains if the interstellar medium (ISM) is enriched with dust (e.g. Cazaux & Tielens 2004; Yamasawa et al. 2011). These effects of dust grains underline the importance of clarifying the dust enrichment and the evolution of dust properties in galaxies.

The evolution of dust in a galaxy is governed by various processes (e.g. Asano et al. 2013a). Dust grains are supplied by stellar sources such as supernovae (SNe) and asymptotic giant branch (AGB) stars (e.g. Bianchi & Schneider 2007; Nozawa et al. 2007; Yasuda & Kozasa 2012). In the Milky Way ISM, the time-scale of dust destruction by SN shocks is a few $\times 10^8$ yr (Jones, Tielens, & Hollenbach 1996; but see Jones & Nuth 2011), which is significantly shorter than the time-scale of dust supply from stellar sources (~ 1.5 Gyr) (McKee 1989). Therefore, it has been argued that dust grains grow in the ISM by the accretion of metals¹ (simply called accretion in this paper) to explain the dust abundance in the ISM in various types of galaxies (Dwek 1998; Zhukovska, Gail, & Trieloff 2008; Draine 2009; Pipino et al. 2011; Valiante et al. 2011; Inoue 2011; Asano et al. 2013b). The most efficient sites of grain growth are molecular clouds, where the typical number density of hydrogen molecules is $\sim 10^3 \text{ cm}^{-3}$ (Hirashita 2000).

* E-mail: hirashita@asiaa.sinica.edu.tw

¹ We call the elements composing grains ‘metals’.

Although accretion is suggested to govern the dust abundance, direct evidence of accretion is still poor. Larger depletion of metal elements in the cold clouds than in the warm medium (Savage & Sembach 1996) may indicate grain growth by accretion in clouds. Voshchinnikov & Henning (2010, hereafter VH10) show that the metals are more depleted on to the dust as the optical extinction curve becomes flatter. The depletion is an indicator of how much fraction of the metals are accreted on the dust, while the flatness of extinction curve reflects the size of dust grains. Thus, their result indicates that the accretion of metals on to dust grains and the growth of grain size occur at the same sites.

Dust grains also grow through coagulation; i.e. grain–grain sticking (e.g. Chokshi, Tielens, & Hollenbach 1993). A deficit of very small grains contributing to the 60- μm emission is observed around a typical density in molecular clouds $\sim 10^3 \text{ cm}^{-3}$, and is interpreted to be a consequence of coagulation (Stepnik et al. 2003). Coagulation efficiently occurs in the dense medium like accretion. Thus, it is reasonable to consider that accretion and coagulation take place at the same time.

Although accretion and coagulation can simultaneously occur, they may have different influences on observational quantities. While accretion changes both the total dust mass and the grain sizes, coagulation only changes the grain sizes, conserving the total dust mass. In the above, we have mentioned the observed relation between depletion and extinction curve by VH10. In interpreting this relation, we should note that the depletion is only affected by accretion while the extinction curve is influenced by both accretion and coagulation. Therefore, there is a possibility of disentangling the effects of accretion and coagulation by interpreting the relation between depletion and extinction curve.

The shape of extinction curve may be capable of discriminating the two grain growth mechanisms, accretion and coagulation (Cardelli, Clayton, & Mathis 1989; O’Donnell & Mathis 1997). Coagulation makes the grain sizes larger and the extinction curve flatter, while accretion increases the extinction itself. Hirashita (2012, hereafter H12) points out a possibility that accretion steepens the extinction curve at ultraviolet (UV) and optical wavelengths. Thus, accretion and coagulation, although these two processes occur simultaneously in the dense ISM, can have different impacts on the extinction curve.

The above arguments are mainly based on qualitative observational evidence or purely theoretical arguments on each of the two processes (accretion and coagulation). Thus, in this paper, we solve the evolution of extinction curve by accretion and coagulation *simultaneously* and compare with some *quantitative* indicators that characterize major features of extinction curve. We also use the metal depletion as an indicator of accretion, to isolate the effect of accretion. As a consequence of this study, we can address if the observed variation of extinction curve is consistent with the grain growth mechanisms and test the widely accepted hypothesis that accretion and coagulation are really occurring in the ISM. We concentrate on the Milky Way ISM, for which detailed data are available for the extinction curves.

This paper is organized as follows. We explain our models used to calculate the effects of accretion and coagulation on the extinction curve in Section 2. We show the calculation results and compare them with the observational data of Milky Way extinction curves and depletion in Section 3. The models are also tested by a large sample of Milky Way extinction curves in Section 4. After discussing some implications of our results in Section 5, we conclude in Section 6.

2 MODELS

We consider the time evolution of grain size distribution by the following two processes: the accretion of metals and the growth by coagulation in an interstellar cloud. These two processes are simply called accretion and coagulation in this paper. Our aim is to investigate if dust grains processed by these processes can explain the variation of extinction curves in various lines of sight. We only treat grains refractory enough to survive after the dispersal of the cloud, and do not consider volatile grains such as water ice. We assume that the grains are spherical with a constant material density s dependent on the grain species, so that the grain mass m and the grain radius a are related as

$$m = \frac{4}{3}\pi a^3 s. \quad (1)$$

We define the grain size distribution such that $n(a, t) da$ is the number density of grains whose radii are between a and $a + da$ at time t . In our numerical scheme, we use the number density of grains with mass between m and $m + dm$, $\tilde{n}(m, t)$, which is related to $n(a, t)$ by $\tilde{n}(m, t) dm = n(a, t) da$; that is, $\tilde{n} = n/(4\pi a^2 s)$. For convenience, we also define the dust mass density, $\rho_d(t)$:

$$\rho_d(t) = \int_0^\infty \frac{4}{3}\pi a^3 s n(a, t) da. \quad (2)$$

The time evolution of grain size distribution by accretion and coagulation is calculated based on the formulation by H12. We consider silicate and carbonaceous dust as grain species. To avoid the complexity in compound species, we treat these two grain species separately. We neglect the effect of the Coulomb interaction on the cross-section (i.e. the cross-section of a grain for accretion and coagulation is simply estimated by the geometric one). For ionized particles, the effect of electric polarization could raise the cross-section especially for small grains (e.g. Draine & Sutin 1987). Therefore, neglecting the Coulomb interaction may lead to an underestimate of grain growth by accretion. However, the ionization degree in dense clouds is extremely low (Yan, Lazarian & Draine 2004), which means that almost all the metal atoms colliding with the dust grains are neutral. For grain–grain collisions, the effect of charring is of minor significance, since the kinetic energy of the grains is much larger than the Coulomb energy at the grain surface. We briefly review the formulation by H12 in the following. Accretion and coagulation, described separately in the following subsections, are solved simultaneously in the calculation.

2.1 Accretion

The equation for the time evolution of grain size distribution by accretion is written as (see H12 for the derivation)

$$\frac{\partial \sigma}{\partial t} + \dot{\mu} \frac{\partial \sigma}{\partial \mu} = \frac{1}{3} \dot{\mu} \sigma, \quad (3)$$

where $\sigma(m, t) \equiv m \tilde{n}(m, t)$, $\mu \equiv \ln m$, and $\dot{\mu} \equiv d\mu/dt$. The time evolution of the logarithmic grain mass μ can be written as

$$\dot{\mu} = \frac{3\xi_X(t)}{\tau(m)}, \quad (4)$$

where $\tau(m)$ is the growth time-scale of grain radius as a function of grain mass (given by equation 5; note that m and a are related by equation 1), and $\xi_X(t) = n_X/n_{X,\text{tot}}$ the gas-phase fraction of key element X ($X = \text{Si}$ and C for silicate and carbonaceous dust, respectively) as a function of time (n_X is the number density of key species X in gas phase as a function of time, and $n_{X,\text{tot}}$ is the

Table 1. Adopted quantities.

Species	X	f_X^a	m_X^b amu	$(X/H)_\odot^c$	s^c (g cm^{-3})
Silicate	Si	0.163	28.1	3.3×10^{-5}	3.5
Graphite	C	1	12	3.63×10^{-4}	2.24

^aFor silicate, we assume a composition of MgFeSiO₄ (Weingartner & Draine 2001).

^bThe atomic masses and the abundances are taken from Cox (2000).

^cWe adopt the same values as those used by Weingartner & Draine (2001) for the models. Although the solar abundance varies among various measurements, such a variation does not affect our conclusions.

number density of element X in both gas and dust phases). The growth time-scale is evaluated as

$$\tau(a) \equiv \frac{a}{\frac{n_{X,\text{tot}} m_X S_{\text{acc}}}{f_X s} \left(\frac{k_B T_{\text{gas}}}{2\pi m_X} \right)^{1/2}}, \quad (5)$$

where m_X is the atomic mass of X, S_{acc} is the sticking probability for accretion, f_X is the mass fraction of the key species in dust, k_B is the Boltzmann constant, and T_{gas} is the gas temperature. The evolution of ξ_X is calculated by

$$\frac{d\xi_X}{dt} = \frac{-3f_X \xi_X(t)}{m_X n_{X,\text{tot}}} \int_0^\infty \frac{\sigma(m, t)}{\tau(m)} dm. \quad (6)$$

We solve equations (3)–(6) to obtain the time evolution of $\sigma(m, t)$, which is translated into $n(a, t)$.

To clarify the time-scale of accretion, we give the numerical estimates for τ . With the values of parameters given in Table 1, $\tau(a)$ in equation (5) can be estimated as

$$\begin{aligned} \tau &= 1.80 \times 10^8 \left(\frac{a}{0.1 \mu\text{m}} \right) \left(\frac{Z}{Z_\odot} \right)^{-1} \left(\frac{n_{\text{H}}}{10^3 \text{ cm}^{-3}} \right)^{-1} \\ &\times \left(\frac{T_{\text{gas}}}{10 \text{ K}} \right)^{-1/2} \left(\frac{S_{\text{acc}}}{0.3} \right)^{-1} \text{ yr} \end{aligned} \quad (7)$$

for silicate, and

$$\begin{aligned} \tau &= 0.993 \times 10^8 \left(\frac{a}{0.1 \mu\text{m}} \right) \left(\frac{Z}{Z_\odot} \right)^{-1} \left(\frac{n_{\text{H}}}{10^3 \text{ cm}^{-3}} \right)^{-1} \\ &\times \left(\frac{T_{\text{gas}}}{10 \text{ K}} \right)^{-1/2} \left(\frac{S_{\text{acc}}}{0.3} \right)^{-1} \text{ yr} \end{aligned} \quad (8)$$

for carbonaceous dust (n_{H} is the number density of hydrogen nuclei). We adopt the same values as those in H12 for the following quantities: $Z = Z_\odot$, $n_{\text{H}} = 10^3 \text{ cm}^{-3}$, $T_{\text{gas}} = 10 \text{ K}$, and $S_{\text{acc}} = 0.3$. Note that the same result is obtained with the same value of $Z n_{\text{H}} S t$; in particular, the density may vary in a wide range, so that it is worth noting that the time-scales of accretion and coagulation both scale with $\propto n_{\text{H}}^{-1}$ (see also Section 5.2).

2.2 Coagulation

We solve a discretized coagulation equation used in Hirashita & Yan (2009). We consider thermal (Brownian) motion and turbulent motion as a function of grain mass (or radius, which is related to the mass by equation 1) (see H12 for details). The size-dependent velocity dispersion of grains is denoted as $v(a)$. The coagulation is assumed to occur if the relative velocity is below the coagulation threshold given by Hirashita & Yan (2009) (see Chokshi, Tielens, & Hollenbach 1993; Dominik & Tielens

1997; Yan, Lazarian & Draine 2004) unless otherwise stated. We modify the treatment of relative velocities following Hirashita & Li (2013): in considering a collision between grains with sizes a_1 and a_2 , we estimate the relative velocity, v_{12} by

$$v_{12} = \sqrt{v(a_1)^2 + v(a_2)^2 - 2v(a_1)v(a_2)\cos\theta}, \quad (9)$$

where θ is the angle between the two grain velocities, and $\cos\theta$ is randomly chosen between -1 and 1 in each time-step. We also assume that the sticking coefficient S_{coag} is 1 unless otherwise stated, also examining models (the tuned model described later) in which S_{coag} is less than 1.

2.3 Initial conditions

We adopt an initial grain size distribution that fits the mean Milky Way extinction curve. Weingartner & Draine (2001) assume the following functional form for the grain size distributions of silicate and carbonaceous dust:

$$\begin{aligned} n(a)/n_{\text{H}} &= \frac{C_i}{a} \left(\frac{a}{a_{t,i}} \right)^{\alpha_i} F(a; \beta_i, a_{t,i}) \\ &\times \begin{cases} 1 & (3.5 \text{ \AA} < a < a_{t,i}); \\ \exp\left\{-[(a - a_{t,i})/a_{c,i}]^3\right\} & (a > a_{t,i}); \end{cases} \end{aligned} \quad (10)$$

where i specifies the grain species ($i = s$ for silicate and $i = g$ for carbonaceous dust, which is assumed to be graphite) and the term

$$F(a; \beta_i, a_{t,i}) \equiv \begin{cases} 1 + \beta a/a_{t,i} & (\beta \geq 0); \\ (1 - \beta a/a_{t,i})^{-1} & (\beta < 0) \end{cases} \quad (11)$$

provides curvature. We omit the log-normal term for small carbonaceous dust (i.e. $b_{\text{C}} = 0$ in Weingartner & Draine 2001), which is dominated by polycyclic aromatic hydrocarbons (PAHs), since it is not clear how PAHs contribute to the accretion and coagulation to form macroscopic grains. Note that Weingartner & Draine (2001) favour $b_{\text{C}} > 0$ based on the observed strong PAH emission from the diffuse ISM (Li & Draine 2001). If PAHs contribute to form macroscopic grains through accretion and coagulation, our estimate gives a conservative estimate for the effect of accretion. However, after coagulation becomes dominant at $\gtrsim 100$ Myr, the existence of PAHs does not affect the results as long as PAHs have a negligible contribution to the total dust mass, which is the case in Weingartner & Draine (2001)'s grain size distributions. The size distribution has five parameters ($C_i, a_{t,i}, a_{c,i}, \alpha_i, \beta_i$) for each grain species. We adopt the solution for $b_{\text{C}} = 0$ and $R_V = 3.1$ (see equation 15 for the definition of R_V) in Weingartner & Draine (2001) to fix these parameters. The adopted values are listed in Table 2.

The initial value of ξ_X is given for each dust species as follows. The dust mass density at $t = 0$, $\rho_d(0)$, is given for silicate and carbonaceous dust separately by equation (2) with the initial grain size distribution (equation 10). As derived in H12, $\rho_d(0)$ is related to the initial condition for ξ_X as

$$\rho_d(0) = \frac{m_X}{f_X} [1 - \xi_X(0)] \left(\frac{Z}{Z_\odot} \right) \left(\frac{X}{\text{H}} \right)_\odot n_{\text{H}}, \quad (12)$$

where Z is the metallicity, (we apply $Z = Z_\odot$ throughout this paper), and $(X/H)_\odot$ is the solar abundance (the ratio of the number of X nuclei to that of hydrogen nuclei at the solar metallicity). With the solar abundances of Si and C (Table 1), we obtain $\xi_{\text{C}}(0) = 0.198$ for carbonaceous dust, while $\xi_{\text{Si}}(0)$ is negative for silicate. This means that too much silicon is used to explain the Milky Way extinction curve by Weingartner & Draine (2001). As

Table 2. Parameter values for the initial grain size distributions.

Species	C_i	$a_{t,i}$ (μm)	$a_{c,i}$ (μm)	α_i	β_i
Silicate	1.02×10^{-12}	0.172	0.1	-1.48	-9.34
Carbonaceous dust	9.94×10^{-11}	0.00745	0.606	-2.25	-0.0648

they mentioned, since there is still an uncertainty in the interstellar elemental abundances, we do not try to adjust the silicon and carbon abundances. In fact, for the purpose of investigating the effects of accretion and coagulation on the extinction curve, fine-tuning of elemental abundance is not essential. Thus, we assume $\xi_{\text{Si}}(0) = 0.1$ as a typical depletion of silicon in the ISM (VH10), while we adopt $\xi_{\text{C}}(0) = 0.198$ as expected from the interstellar carbon abundance.

2.4 Calculation of extinction curves

Extinction curves are calculated by adopting the method described by Weingartner & Draine (2001). The extinction at wavelength λ in units of magnitude (A_λ) normalized to the column density of hydrogen nuclei (N_{H}) is written as

$$\frac{A_\lambda(t)}{N_{\text{H}}} = \frac{2.5 \log e}{n_{\text{H}}} \int_0^\infty da n(a, t) \pi a^2 Q_{\text{ext}}(a, \lambda), \quad (13)$$

where $Q_{\text{ext}}(a, \lambda)$ is the extinction efficiency factor, which is evaluated by using the Mie theory (Bohren & Huffman 1983). For the details of optical constants for silicate and carbonaceous dust, see Weingartner & Draine (2001). The colour excess at wavelength λ is defined as

$$E(\lambda - V) \equiv A_\lambda - A_V, \quad (14)$$

where the wavelength at the V band is $0.55 \mu\text{m}$. The steepness of extinction curve is often quantified by R_V :

$$R_V \equiv \frac{A_V}{E(B - V)}, \quad (15)$$

where the wavelength at the B band is $0.44 \mu\text{m}$. Since a flat extinction curve decreases the difference between A_V and A_B [i.e. $E(B - V)$], R_V increases as the extinction curve becomes flatter.

To extract some features in UV extinction curves, we apply a parametric fit to the calculated extinction curves according to Fitzpatrick & Massa (2007). They adopt the following form for $\lambda \leq 2700 \text{ \AA}$:

$$\begin{aligned} & E(\lambda - V)/E(V - B) \\ &= \begin{cases} c_1 + c_2 x + c_3 D(x, x_0, \gamma) & (x \leq c_5), \\ c_1 + c_2 x + c_3 D(x, x_0, \gamma) + c_4 (x - c_5)^2 & (x > c_5), \end{cases} \end{aligned} \quad (16)$$

where $x \equiv \lambda^{-1} (\mu\text{m}^{-1})$, and

$$D(x, x_0, \gamma) = \frac{x^2}{(x^2 - x_0^2)^2 + x^2 \gamma^2} \quad (17)$$

is introduced to express the 2175- \AA bump (carbon bump). There are seven parameters, $(c_1, \dots, c_5, x_0, \gamma)$. To stabilize the fitting, we fix $c_5 = 6.097$, $x_0 = 4.592 \mu\text{m}^{-1}$, and $\gamma = 0.922 \mu\text{m}^{-1}$ by adopting the values fitting to the mean extinction curve in the Milky Way (Fitzpatrick & Massa 2007). The ranges of these parameters are narrow compared with the other parameters. We apply a least-square fitting to the theoretically predicted extinction curves to derive (c_1, \dots, c_4) .

It is observationally suggested that there is a link between UV extinction and R_V (Cardelli et al. 1989) although the scatter is large (Fitzpatrick & Massa 2007). The carbon bump strength has also a weak correlation with R_V in such a way that the bump is smaller for a flatter extinction curve (larger R_V) (Cardelli et al. 1989; Fitzpatrick & Massa 2007). We examine if these relations are consistent with accretion and coagulation. To estimate the bump strength, we introduce the following two quantities: $A_{\text{bump}} \equiv \pi c_3 / (2\gamma)$ and $E_{\text{bump}} \equiv c_3 / \gamma^2$ (note that A_{bump} and E_{bump} are simply determined by c_3 after fixing γ). If an extinction curve is steep in the optical it tends to be steep also in the UV. This is reflected in the correlation between R_V and c_2 (c_2 is the slope of UV extinction curve at both sides of the carbon bump). Following Fitzpatrick & Massa (2007), we also define a far-UV (FUV) curvature as $\Delta 1250 \equiv c_4 (8.0 - c_5)^2$.

2.5 Data

We test the change of grain size distribution by accretion and coagulation through the comparison of our models with observational extinction and depletion data compiled by VH10 for stars located in the Scorpius-Ophiuchus region, since the data covers a wide range in R_V . There are 7 stars (HD 143275, HD 144217, HD 144470, HD 147165, HD 147888, HD 147933, and HD 148184): for these stars, Mg or Si abundance in the line of sight is measured. The depletion derived from the metal abundance measurements is crucial to separate the effect of accretion. Among the 7 stars, extinction curves are available for 4 stars (HD 144470, HD 147165, HD 147888, and HD 147933) (Voshchinnikov 2012).

We also use a larger sample compiled by Fitzpatrick & Massa (2007), although they do not have metal abundance data. They compiled UV-to-near-infrared extinction data for Galactic 328 stars. In particular, some important parameters that characterize the extinction curve (A_{bump} , E_{bump} , c_2 , and $\Delta 1250$) are available, so that we can check if the change of extinction curve by accretion and coagulation is consistent with the observed trend or range of these parameters for various R_V .

3 RESULTS

3.1 Extinction curves

3.1.1 General behaviour of theoretical predictions

We show the evolution of grain size distribution in Fig. 1 for silicate and carbonaceous dust. To show the mass distribution per logarithmic size, we multiply a^4 to n . The details about how accretion and coagulation contribute to the grain size distribution have already been discussed in H12. We briefly overview the behaviour.

Since the growth rate of grain radius by accretion is independent of a (H12), the impact of grain growth is significant at small grain sizes. Moreover, almost all gas-phase metals accrete selectively on to small grains because the contribution to

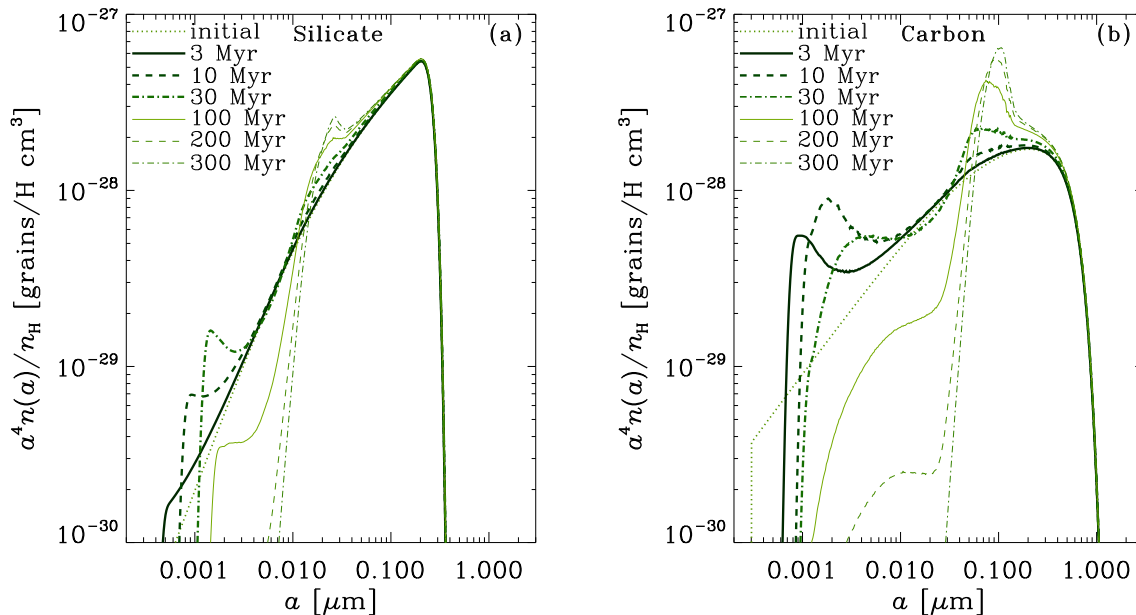


Figure 1. Evolution of grain size distribution for (a) silicate and (b) carbonaceous dust. The grain size distribution is normalized to the hydrogen number density and multiplied by a^4 to show the mass distribution per logarithmic grain radius bin. The thick solid, thick dashed, thick dot-dashed, thin solid, thin dashed, and thin dot-dashed lines show the grain size distributions at $t = 3, 10, 30, 100, 200$ and 300 Myr, respectively. The initial condition is shown by the dotted line.

the grain surface is the largest at the smallest sizes (see also Weingartner & Draine 1999). Since the accretion time-scale for the smallest grains ($a \sim 0.001 \mu\text{m}$) is short, the effect of accretion appears at first, enhancing the grain abundance at the smallest sizes. Accretion stops after the gas-phase elements composing the dust are used up ($\sim 10\text{--}30$ Myr). After accretion stops, the evolution of grain size distribution is driven by coagulation. Coagulation occurs in a bottom-up manner, because small grains dominate the total grain surface. Moreover, the grains at the largest sizes are intact because they have velocities larger than coagulation threshold.

Based on the grain size distributions shown above, we calculate the evolution of extinction curve. In Fig. 2a, we show the extinction curves (A_λ/N_H , calculated by equation 13) for various t . To show that the initial condition reproduces the mean extinction curve, we also plot the averaged extinction curve taken from Pei (1992) (the shape is almost identical to Fitzpatrick & Massa (2007)’s mean extinction curve). We also show in Fig. 2b the normalized colour excess, $E(\lambda - V)/E(B - V)$. In the bottom panels of those two figures, we present all the curves divided by the initial values to indicate how the steepness of extinction curve changes as a function of time.

In Fig. 2a, we observe that the extinction increases at all wavelengths at $t \lesssim 10$ Myr because accretion increases the dust abundance. The extinction normalized to the value at $t = 0$ [$A_\lambda/A_\lambda(0)$] increases toward shorter wavelengths at $t \lesssim 10$ Myr, indicating that accretion steepens the UV extinction curve. This is because the UV extinction responds more sensitively to the increase of the grains at $a \sim 0.001\text{--}0.01 \mu\text{m}$ by accretion than the optical–near-infrared extinction (see also H12). After that, coagulation makes the grains larger (Fig. 1), decreasing the UV extinction and flattening the extinction curve. The optical–near-infrared extinction continues to increase even after ~ 10 Myr because the increase of grain sizes by coagulation increases the grain opacity in the optical

and near-infrared. The carbon ($2175\text{-}\text{\AA}$) bump, which is produced by small ($a \lesssim 300 \text{\AA}$; Draine & Lee 1984) carbonaceous grains, become less prominent as coagulation proceeds, because small carbonaceous grains responsible for the bump are depleted after coagulation.

The normalized colour excesses shown in Fig. 2b naturally follow the same behaviour as in Fig. 2a. From the bottom panel in Fig. 2b, we observe that the ratio is > 1 at wavelengths shorter than $0.44 \mu\text{m}$ while accretion dominates ($t \lesssim 10$ Myr); and that it is < 1 after coagulation takes place significantly. This behaviour confirms that accretion first makes the extinction curve steep and coagulation then modifies it in the opposite way (see also H12). The increase of R_V by coagulation is also reflected in the increase of the absolute value of the intercept, $-\lim_{1/\lambda \rightarrow +0} E(\lambda - V)/E(B - V) = R_V$.

3.1.2 Comparison with observed extinction curves

For our sample (Section 2.5), extinction curves are available for four stars. These extinction curves are shown in Fig. 3. Even for large R_V , the carbon bump around $0.22 \mu\text{m}$ is clear and the UV extinction rises with a positive curvature. However, our theoretical predictions shown in Fig. 2 indicate that at large R_V (i.e. after significant coagulation at > 100 Myr), the carbon bump disappears. This implies that coagulation is in reality not so efficient as assumed in the model for carbonaceous dust. There is another discrepancy: the observed A_V/N_H tends to decrease significantly as R_V increases, while it does not decrease significantly after significant coagulation at > 100 Myr, except at the carbon bump. This is because silicate stops to coagulate at $a \sim 0.03 \mu\text{m}$, which is still too small to affect the UV opacity.

In summary, the observational data indicates (i) that carbonaceous dust should be more inefficient in coagulation than assumed, and (ii) that silicate should grow beyond $a \sim 0.03 \mu\text{m}$ (the growth

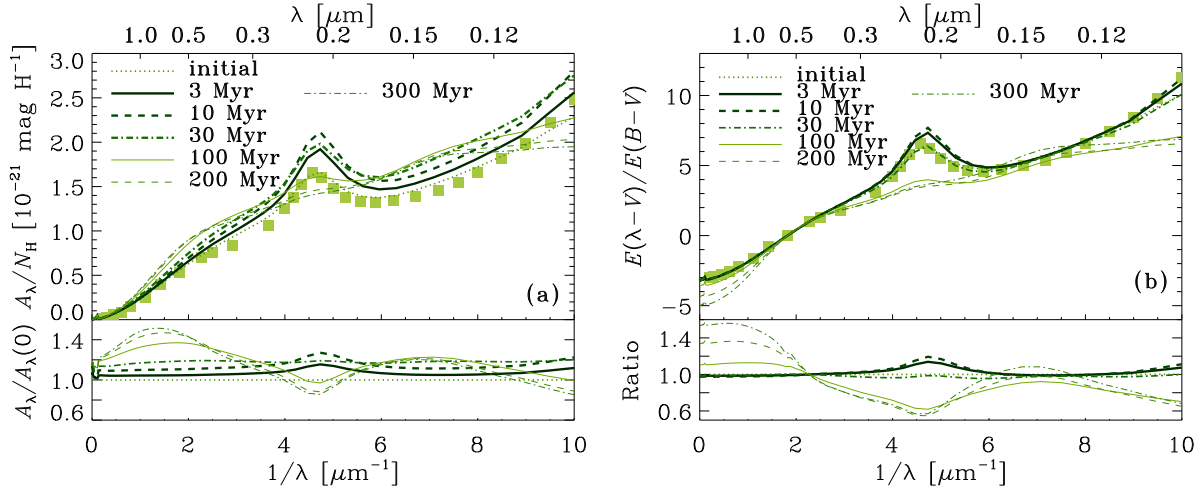


Figure 2. Evolution of extinction curves. We show (a) A_λ/N_H , and (b) $E(\lambda - V)/E(B - V)$. The dotted line is the initial extinction curve before accretion and coagulation. The thick solid, thick dashed, thin solid, thin dashed, and thin dot-dashed lines show the grain size distributions at $t = 3, 10, 30, 100, 200,$ and 300 Myr, respectively. The filled squares represent the mean Milky Way extinction data taken from Pei (1992) as a reference. In each panel, the lower window shows the extinction divided by the initial extinction (the correspondence between the line types and the models is the same as above). The values of R_V are 3.26, 3.21, 3.17, 3.20, 3.59, 4.36, and 5.00 at $t = 0, 3, 10, 30, 100, 200,$ and 300 Myr, respectively.

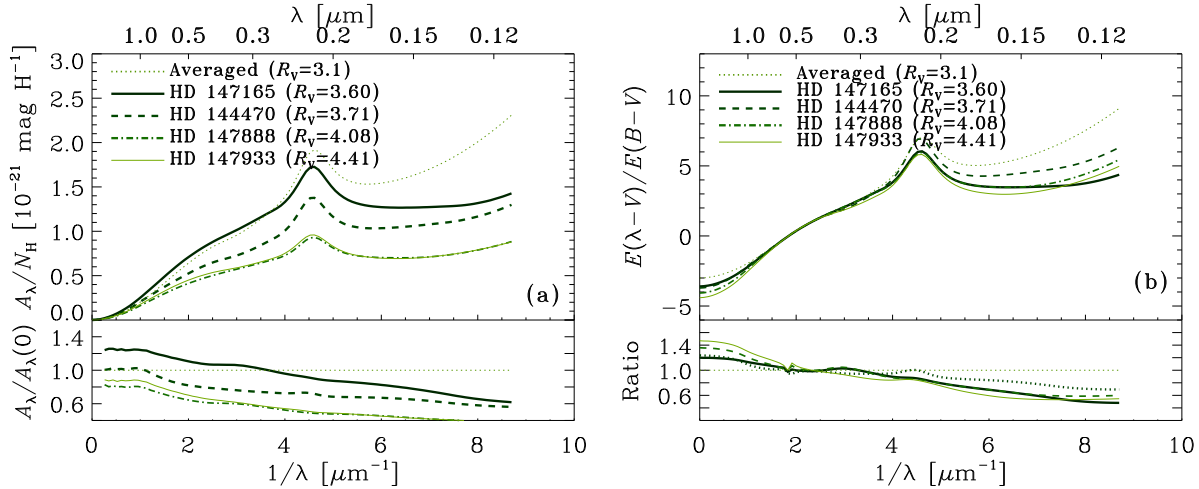


Figure 3. Observed extinction curves for our sample. We show (a) extinction curves in units of magnitude per hydrogen, A_λ/N_H , and (b) normalized colour excess, $E(\lambda - V)/E(B - V)$. The thick solid, dashed, dot-dashed, and thin solid lines show the extinction curves for HD 147165, HD 144470, HD 147888, and HD 147933, respectively. The dotted line represents the averaged Milky Way curve for reference. The R_V values are also indicated. In each panel, the lower window shows the extinction divided by the averaged extinction (the correspondence between the line types and the objects is the same as above).

is limited by the coagulation threshold velocity). Therefore, we also try models with $S_{\text{coag}} < 1$ for carbonaceous dust and no coagulation threshold for silicate dust as a tuned model described in the next subsection.

3.2 Tuned model

Based on the comparisons with observational data in the above, we propose the following tuning for the model. Since the coagulation of carbonaceous dust proves to be too efficient, we decrease the coagulation efficiency by a factor of 2 by adopting $S_{\text{coag}} = 0.5$ for carbonaceous dust, while we keep using $S_{\text{coag}} = 1$ for silicate. For silicate, we get rid of the coagulation threshold; that is, silicate grains are assumed to coagulate whenever they collide. Indeed, if

we consider fluffiness of coagulated grains, the structure can efficiently absorb the energy in collision and large grain can be formed after sticking (Ormel et al. 2009). We do not change the accretion efficiency ($S_{\text{acc}} = 0.3$) for both silicate and carbonaceous dust to minimize the fine tuning. This is called ‘tuned model’, while we call the original model with $S_{\text{coag}} = 1$ and the coagulation threshold ‘original model without tuning’. As shown later, such a minimum tuning of the original model is enough to explain the variation of main extinction curve features. We do not tune accretion since the final result is only sensitive to the relative efficiencies of accretion and coagulation (so we only tune coagulation to avoid the degeneracy).

The evolution of grain size distribution for the tuned model is shown in Fig. 4. For silicate, compared with the dust distributions

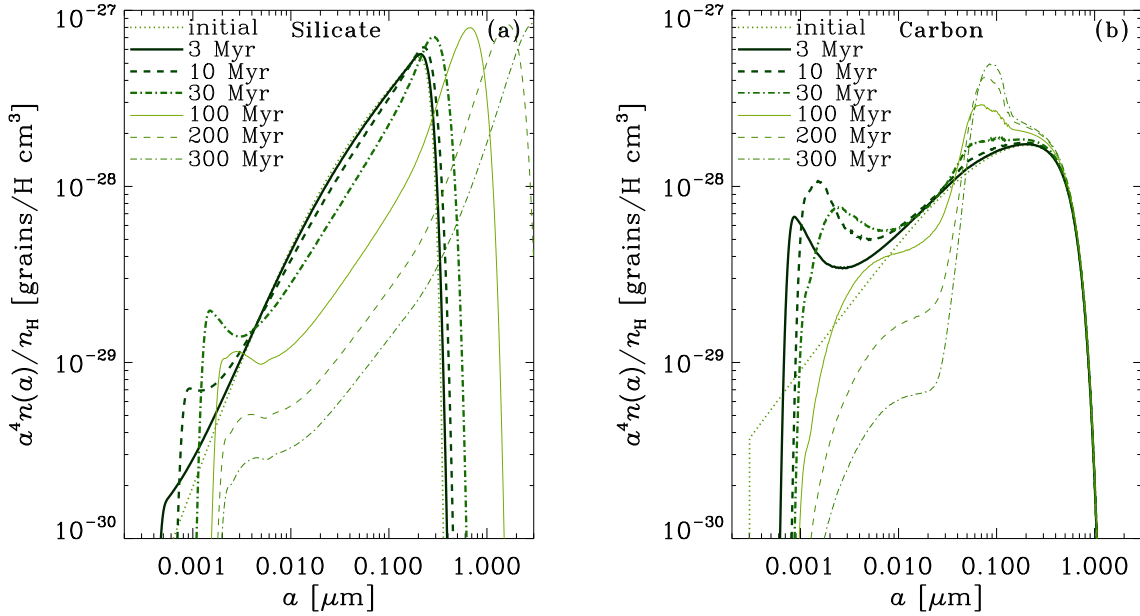


Figure 4. Same as Fig. 1 but for the tuned model.

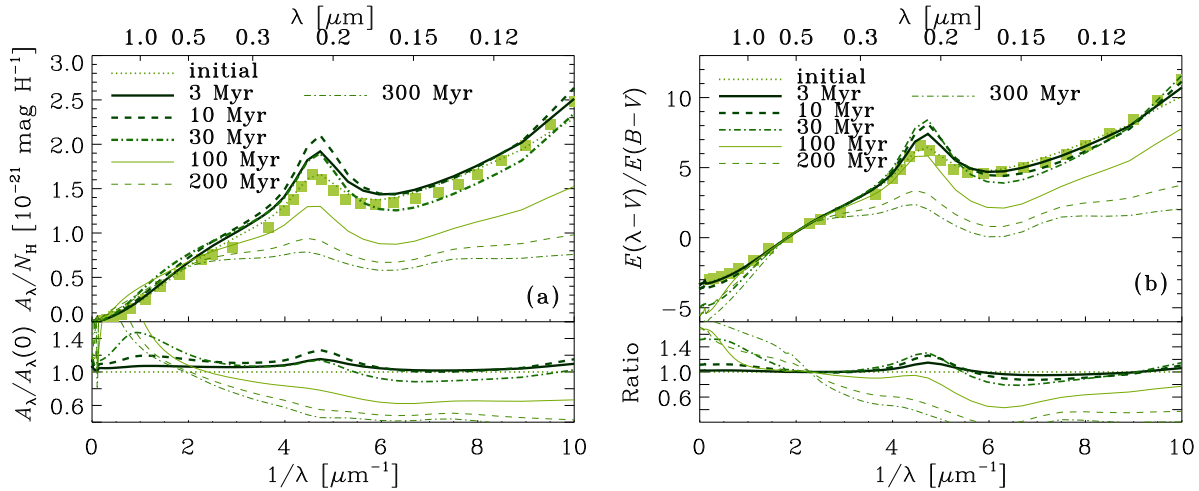


Figure 5. Same as Fig. 2 but for the tuned model. The values of R_V are 3.26, 3.33, 3.63, 4.94, 5.48, 5.56, and 6.40 at $t = 0, 3, 10, 30, 100, 200,$ and 300 Myr, respectively.

in the original model without tuning (Fig. 1), the grains grow further, even beyond $0.2 \mu\text{m}$ at > 100 Myr. This is simply because we removed the coagulation threshold so that the grains can coagulate at any velocities. For carbonaceous dust, the effect of tuning slightly increases the abundance of small grains ($\lesssim 300 \text{ \AA}$) that can contribute to the carbon bump, although the change is not so drastic as for silicate. Nevertheless, we will show later that such a small change has a significant impact on the strength of carbon bump.

Fig. 5 shows the extinction curves for the tuned model. A_V/N_H decreases at > 30 Myr when $R_V \gtrsim 5$. This is consistent with the observed trend that A_V/N_H decreases as R_V increases (Fig. 3). This decrease is particularly driven by coagulation of silicate grains. The tuned model also keeps the bump strong even at later epochs, which is also consistent with the observed extinction

curves. The more prominent carbon bump in the tuned model than in the original model without tuning is due to slower coagulation of carbonaceous dust. For $E(\lambda - V)/E(B - V)$, the variation of observed UV extinction curves in Fig. 3, compared with that of theoretical ones in Fig. 5, can be interpreted as the flattening at $\gtrsim 30$ Myr by coagulation.

3.3 Relation between depletion and R_V

VH10 use $1 - \xi_X$ (in their notation $1 - D_X$) to quantify the fraction of element X condensed into dust grains. In particular, they show that $1 - \xi_X$ has a correlation with the shape of extinction curve. As mentioned in Section 2.4, we adopt R_V as a representative quantity for the extinction curve slope. VH10 focus on silicate. Since

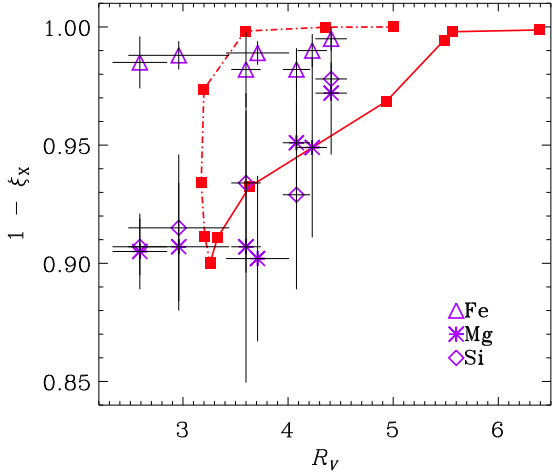


Figure 6. Relation between $1 - \xi_X$ (the fraction of element of X in dust phase) and R_V (in the extinction curve) at 0, 3, 10, 30, 100, 200, and 300 Myr for increasing $1 - \xi_X$. The filled squares connected with the solid and dashed lines show the theoretical results for the tuned model and the original model without tuning. The triangles, asterisks, and diamonds are the data taken from VH10 for X = Fe, Mg, and Si (in the models we adopt Si for the tracer element).

we adopted Si as a key element of silicate, we concentrate on the relation between $1 - \xi_{\text{Si}}$ and R_V (note that R_V is also affected by carbonaceous dust as well as silicate). In Fig. 6, we compare the relations calculated by the models with the observational data (we also plot the observed depletions of Fe and Mg as references).

First, we discuss the original model without tuning shown by the dashed line in Fig. 6. The slight decrease of R_V at $\lesssim 10$ Myr is due to accretion. Accretion increases $1 - \xi_X$ rapidly in 30 Myr. After 30 Myr, coagulation increases R_V as the extinction curve becomes flat. As a result, $1 - \xi_X$ increases (and R_V decreases slightly) before R_V increases. This behaviour on the $(1 - \xi_X)$ - R_V diagram does not explain the observed positive correlation between these two quantities in Fig. 6. The discrepancy implies that accretion proceeds too quickly compared with coagulation in the original model without tuning.

Next, we examine the tuned model. Note that the tuning is meant to reproduce the observed trend in extinction curves so it is not obvious if it reproduces the observed relation between depletion and R_V . As is clear from Fig. 6, the tuned model is consistent with the observed trend. This is because of more efficient coagulation of silicate, which pushes R_V to larger values at earlier epochs. Therefore, the tuned model reproduces the observed relation between depletion and R_V .

4 CORRELATIONS AMONG VARIOUS EXTINCTION PROPERTIES

Now we discuss the models in the context of the largest sample of Milky Way extinction curves taken by Fitzpatrick & Massa (2007). Cardelli et al. (1989) suggest that R_V correlates with UV slope and carbon bump strength. More recently, Fitzpatrick & Massa (2007) show that the correlation is not significant for the bulk of the sample with $2.4 < R_V < 3.6$ but that there is a slight trend if data points with larger R_V values are included (see also below). We examine if these weak correlations reflect the evolution of grain size distri-

bution by accretion and coagulation. More precisely, since the correlations are weak, we check if the models are consistent with the observed range of those parameters. As mentioned in Section 2.4, we examine c_2 , Δ_{1250} , A_{bump} , and E_{bump} as characteristic quantities in the extinction curve.

In Fig. 7, we show the relation between each of these parameters (c_2 , Δ_{1250} , A_{bump} , or E_{bump}) and R_V . For the observational data, the stars at > 1 kpc (called distant sample) and < 1 kpc (called nearby sample) are shown in different symbols. For all those parameters, the dispersion is smaller for the distant sample than for the nearby sample. This indicates that the peculiarity in each individual line of sight is reflected more in the nearby sample while the peculiarity is ‘averaged’ for the distant sample. Even for the distant sample, some trends still remain: c_2 and the carbon bump strength both have negative correlations with R_V , although the correlations are weak. The UV curvature has a weak positive trend with R_V for $R_V > 3.5$, although there also seems to be an overall negative trend if we also include the data with smaller R_V . Because of the large variety in individual lines of sight and the weakness of the trend, we only use the relations in Fig. 7 as a reference for our models and do not attempt a fit to the data. Although the initial condition may vary, we simply adopt the same models used above, that is, the original model without tuning and the tuned model with the initial condition described in Section 2.3, in order to focus on the trend produced by accretion and coagulation.

For the UV slope, c_2 , the original model without tuning predicts increasing c_2 (i.e. steepening of the UV extinction curve) for increasing R_V although as shown in Fig. 2, coagulation tends to flatten the overall UV extinction curve. As mentioned in Section 2.4, c_2 reflects the slope around the carbon bump. We find that $E(\lambda - V)/E(B - V)$ decreases around $1/\lambda \sim 4 \mu\text{m}^{-1}$ while it changes little around $1/\lambda \sim 6 \mu\text{m}^{-1}$ in the original model without tuning. The decrease around $1/\lambda \sim 4 \mu\text{m}^{-1}$ is due to the flattening of carbon extinction curve. On the other hand, silicate extinction changes insignificantly since the silicate abundance at $a > 0.03 \mu\text{m}$, where the effects on c_2 is the largest, is little affected by coagulation (because their velocities are larger than the coagulation threshold), so the extinction around $1/\lambda \sim 6 \mu\text{m}^{-1}$, which is dominated by silicate, does not change much. Thus, the extinction curve seems to steepen in terms of c_2 . The tuned model seems to better reproduce the decreasing trend of c_2 for increasing R_V .

For the FUV curvature, Δ_{1250} , we reproduce the observed trend of decreasing Δ_{1250} for increasing R_V (Fig. 7b) with the original model without tuning. However, after 100 Myr, Δ_{1250} becomes negative, which reflects the convex shape at $1/\lambda > 6 \mu\text{m}^{-1}$. No Milky Way extinction curve shows negative Δ_{1250} . The tuned model is rather near to the observational data points.

Also for the bump strengths indicated by A_{bump} and E_{bump} , the original model without tuning can explain the trend of a less prominent bump for a larger R_V . However, the bump weakens too much: Fig. 2 shows that the bump eventually disappears after 100 Myr, which is not consistent with the fact that an extinction curve without carbon (2175-Å) bump is never observed in the Milky Way. The tuned model keeps the bump strong as we observe in Fig. 5. The more prominent carbon bump in the tuned model than in the original model without tuning is due to slower coagulation of carbonaceous dust. The enhancement of the bump by accretion at $t \lesssim 10$ Myr, which may reproduce the upward scatter in the bump strengths, is also worth noting. However, this enhancement causes too large bump strengths around $R_V \sim 5$, although it is interesting that the data points around $R_V > 5.5$ are again reproduced by the

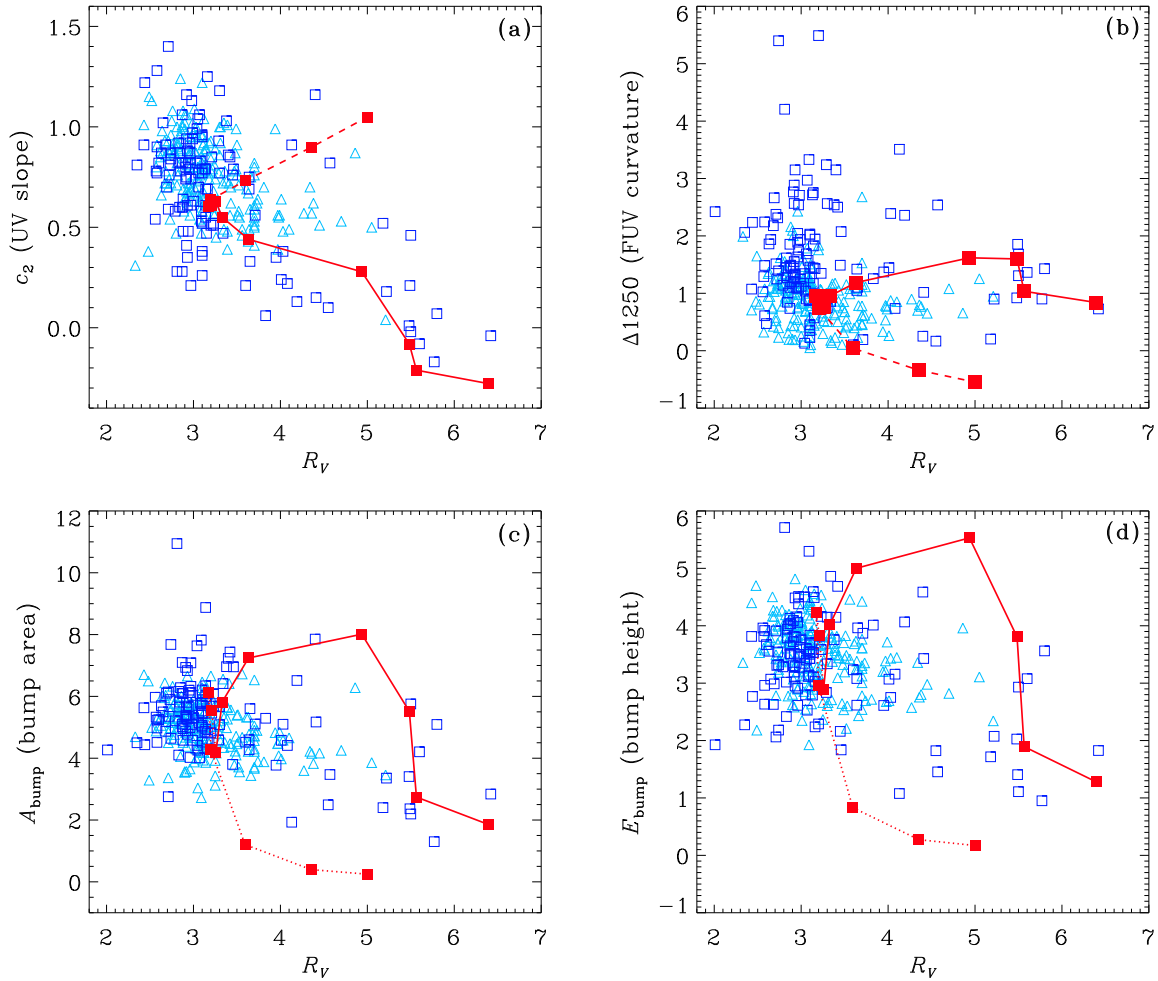


Figure 7. Relation between R_V and each of the characteristic parameters of extinction curve (c_2 , Δ_{1250} , A_{bump} , and E_{bump} in Panels a, b, c, and d, respectively). Our theoretical results are shown by the filled squares connected with lines at $t = 0, 3, 10, 30, 100, 200,$ and 300 Myr (the dashed and solid lines correspond to the original model without tuning and the tuned model, respectively). The evolution starts with the point with $R_V = 3.2$. The points for $t = 3, 10,$ and 30 Myr on the original model without tuning in Panels a and b are almost identical to the point at $t = 0$ Myr. The data points (open triangles and open squares for stars at > 1 kpc and < 1 kpc, respectively) derived from extinction curves in the Milky Way are taken from Fitzpatrick & Massa (2007).

tuned model. The implication is that the scatter of the observational data can reflect the strong dependence on coagulation efficiency, which may be changed by the detailed material properties of dust. We emphasize that only a factor of two variation in S_{coag} (0.5 and 1) easily cover the observed range of bump strength.

5 DISCUSSION

5.1 Implications of the tuned model

In the tuned model, the coagulation threshold of silicate is removed, since the stop of coagulation at small sizes prevents the extinction curve from becoming flat enough to explain the observed UV extinction curves for large R_V . The coagulation efficiency of carbonaceous dust is reduced (only) by a factor of 2 (i.e. we adopted $S_{\text{coag}} = 0.5$) to keep enough abundance of small carbonaceous grains contributing to the carbon bump. Those changes are already enough to reproduce the observational trend in the shape of extinction curves for increasing R_V . The UV slope, the FUV curvature and the carbon bump strength have weak correlations with R_V . The

original model without tuning and the tuned model predict very different tracks in the relations between R_V and each of those quantities. This implies that the large scatters of those quantities in the observational data is due to the sensitive response to the material properties (in our models, the coagulation efficiency).

5.2 Lifetime of molecular clouds

In this paper, we adopted the duration of accretion and coagulation up to 300 Myr. This may be long as a lifetime of molecular clouds (e.g. Lada, Lombardi, & Alves 2010), but Koda et al. (2009) suggest a possibility that molecular clouds are sustained over the circular time-scale in a spiral galaxy (~ 100 Myr). Thus, it is worth investigating such a long duration as a few hundreds of mega-years for accretion and coagulation in molecular clouds.

The duration t is also degenerate with $n_{\text{H}}Z$ as mentioned in Section 2 in such a way that the same value of $tn_{\text{H}}Z$ returns the same result. For example, if we adopt $n_{\text{H}} = 10^4 \text{ cm}^{-3}$ instead of 10^3 cm^{-3} , $R_V \sim 5$ is reached at $t \sim 10$ Myr. However, the tracks on the diagrams shown in Figs. 6 and 7 do not change even

if we change $n_{\text{H}}Z$. In other words, our predictions on the theoretical tracks in these diagram are robust against the variation of gas density.

6 CONCLUSION

We have examined the effects of two major growth mechanisms of dust grains, accretion and coagulation, on the extinction curve. First we examined the evolution of extinction curve by using the prescription for accretion and coagulation with commonly used material parameters. The observational Milky Way extinction curves are not reproduced in the following two respects: (i) The extinction normalized to the hydrogen column density (A_V/N_{H}) does not decrease around $1/\lambda \sim 6\text{--}8 \mu\text{m}^{-1}$ in the model even for large $R_V (> 4)$. (ii) The carbon bump is too small when $R_V > 4$. These two discrepancies are resolved by the following prescriptions (tuning): more efficient coagulation for silicate by removing the coagulation threshold velocity, and less efficient coagulation for carbonaceous dust by a factor of 2. This ‘tuned’ model also reproduces the trend between depletion and R_V , which implies that the time-scale of coagulation relative to that of accretion is appropriate. On the other hand, the original model without tuning fails to reproduce the observed trend between depletion and R_V since too quick accretion relative to coagulation increases depletion even before coagulation increases R_V .

We have also examined the relation between R_V and each of the following extinction curve features: the UV slope, the FUV curvature, and the carbon bump strength. The correlation between the UV slope and R_V , which is the strongest among those three correlations, is well reproduced by the tuned model. For the FUV curvature and the carbon bump, the observational data are located between the original model without tuning and the tuned model, which implies that the scatters in the observational data can be attributed to the sensitive variation to the dust properties (coagulation efficiency in our models). This also means that the variation of extinction curves in the Milky Way, especially at $R_V > 3$, can be interpreted by the variation of grain size distribution by accretion and coagulation. For more complete understanding, especially at $R_V < 3$, other dust processing mechanisms such as shattering should be included.

ACKNOWLEDGMENTS

HH thanks the support from NSC grant NSC102-2119-M-001-006-MY3, and NVV acknowledges the support from the Grant RFBR 13-02- 00138a.

REFERENCES

- Asano, R., Takeuchi, T. T., Hirashita, H., & Nozawa, T. 2013a, *MNRAS*, 432, 637
- Asano, R., Takeuchi, T. T., Hirashita, H., & Inoue, A. K. 2013b, *Earth Planets Space*, 65, 213
- Bianchi, R., & Schneider, R. 2007, *MNRAS*, 378, 973
- Bohren C. F., Huffman D. R., 1983, *Absorption and Scattering of Light by Small Particles*. Wiley, New York
- Cardelli J. A., Clayton G. C., Mathis J. S., 1989, *ApJ*, 345, 245
- Cazaux, S., & Tielens, A. G. G. M. 2004, *ApJ*, 604, 222
- Chokshi, A., Tielens, A. G. G. M., & Hollenbach, D. 1993, *ApJ*, 407, 806
- Cox, A. N. 2000, *Allen’s Astrophysical Quantities*, 4th ed., Springer, New York
- Désert, F.-X., Boulanger, F., & Puget, J. L. 1990, *A&A*, 237, 215
- Dominik, C., & Tielens, A. G. G. M. 1997, *ApJ*, 480, 647
- Draine B. T., 2009, in Henning Th., Grün E., Steinacker J., eds, *ASP Conf. Ser. 414, Cosmic Dust – Near and Far*. Astron. Soc. Pac., San Francisco, p. 453
- Draine, B. T., & Lee, H. M. 1984, *ApJ*, 285, 89
- Draine, B. T., & Sutin, B. 1987, *ApJ*, 320, 803
- Dwek E., 1998, *ApJ*, 501, 643
- Fitzpatrick, E. L., & Massa, D. 2007, *ApJ*, 663, 320
- Hirashita H., 2000, *PASJ*, 52, 585
- Hirashita, H. 2012, *MNRAS*, 422, 1263 (H12)
- Hirashita, H., & Li, Z.-Y. 2013, *MNRAS*, 434, L70
- Hirashita, H., & Yan, H. 2009, *MNRAS*, 394, 1061
- Inoue, A. K. 2011, *Earth, Planets Space*, 63, 1027
- Jones, A. P., & Nuth, J. A., III 2011, *A&A*, 530, A44
- Jones, A. P., Tielens, A. G. G. M., & Hollenbach, D. J. 1996, *ApJ*, 469, 740
- Jones, A. P., Tielens, A. G. G. M., Hollenbach, D. J., & McKee, C. F. 1994, *ApJ*, 433, 797
- Koda, J., et al. 2009, *ApJ*, 700, L132
- Lada, C. J., Lombardi, M., & Alves, J. F. 2010, *ApJ*, 724, 687
- Li, A., & Draine, B. T. 2001, *ApJ*, 554, 778
- McKee, C. F. 1989, in Allamandola L. J. & Tielens A. G. G. M. eds., *IAU Symp. 135, Interstellar Dust*, Kluwer, Dordrecht, 431
- Nozawa, T., Kozasa, T., Habe, A., Dwek, E., Umeda, H., Tomimaga, N., Maeda, K., & Nomoto, K. 2007, *ApJ*, 666, 955
- O’Donnell, J. E., & Mathis, J. S. 1997, *ApJ*, 479, 806
- Ormel, C. W., Paszun, D., Dominik, C., & Tielens, A. G. G. M. 2009, *A&A*, 502, 845
- Pei Y. C., 1992, *ApJ*, 395, 130
- Pipino A., Fan X. L., Matteucci, F., Calura F., Silva L., Granato G., Maiolino R., 2011, *A&A*, 525, A61
- Savage B. D., Sembach K. R., 1996, *ARA&A*, 34, 279
- Stepnik B. et al., 2003, *A&A*, 398, 551
- Valiante, R., Schneider, R., Salvadori, S., & Bianchi, S. 2011, *MNRAS*, 416, 1916
- Voshchinnikov, N. V. 2012, *Journal of Quantitative Spectroscopy & Radiative Transfer*, 113, 2334
- Voshchinnikov, N. V., & Henning, Th. 2010, *A&A*, 517, A45 (VH10)
- Weingartner, J. C., & Draine, B. T. 1999, *ApJ*, 517, 292
- Weingartner, J. C., & Draine, B. T. 2001, *ApJ*, 548, 296
- Yamasawa, D., Habe, A., Kozasa, T., Nozawa, T., Hirashita, H., Umeda, H., & Nomoto, K. 2011, *ApJ*, 735, 44
- Yan H., Lazarian A., Draine B. T., 2004, *ApJ*, 616, 895
- Yasuda, Y., & Kozasa, T. 2012, *ApJ*, 745, 159
- Zhukovska S., Gail H.-P., Tieloff M., 2008, *A&A*, 479, 453

This paper has been typeset from a $\text{\TeX}/\text{\LaTeX}$ file prepared by the author.